Tectonophysics 475 (2009) 423–437

Contents lists available at ScienceDirect

Tectonophysics

journal homepage: www.elsevier.com/locate/tecto

Crustal structure across the Three Gorges area of the Yangtze platform, central China, from seismic refraction/wide-angle reflection data

Zhongjie Zhang [a,*], Zhiming Bai [a], Walter Mooney [b], Chunyong Wang [c], Xuebo Chen [d], Erchie Wang [a], Jiwen Teng [a], Nihal Okaya [b]

[a] State Key Laboratory of Lithospheric Evolution, Institute of Geology and Geophysics, Chinese Academy of Sciences, Beijing, 100029, China
[b] USGS, 345 Middlefield Road, MS 870, Menlo Park, CA 94025, United States
[c] Institute of Geophysics, China Earthquake Administration, Beijing, 100080, China
[d] Institute of Dynamic Deformation, China Earthquake Administration, Beijing, 100081, China

ARTICLE INFO

Article history:
Received 5 November 2007
Received in revised form 11 May 2009
Accepted 24 May 2009
Available online 2 June 2009

Keywords:
Yangtze platform
Zigui basin
Huangling dome
Jianghan basin
P-wave velocities
Composition

ABSTRACT

We present active-source seismic data recorded along a 300 km-long profile across the Three Gorges area of the western Yangtze platform, central China. From west to east, the profile crosses the Zigui basin, Huangling dome and Jianghan basin. The derived crustal *P*-wave velocity structure changes significantly across the Tongchenghe fault that lies at the transition from the Huangling dome to the Jianghan basin. West of the Tongchenghe fault, beneath the Zigui basin and the Huangling dome, we observe a ~42 km thick crust of relatively low average velocity (6.3–6.4 km/s). In contrast, east of the Tongchenghe fault, beneath the Jianghan basin, the crust is only 30 km thick and has a high average velocity (6.6–6.7 km/s). A west–east variation in crustal composition along the Tongchenghe fault is also inferred. West of the fault, *P*-wave velocities suggest a felsic composition with an intermediate layer at the base of the crust, whilst, east of the fault, felsic, intermediate, and mafic crustal layers are apparent. Our results suggest that the crust beneath the Jianghan basin has been thinned by rifting, accompanied by intrusion of the lower crust by mafic dikes and sills. The west-to-east division of the crust in the Three Gorges area coincides with first-order geophysical contrasts in gravity, topography, crustal and lithospheric thickness.

1. Introduction

The Three Gorges area seismic profile is located at ~30°N and ~110°E on the western Yangtze platform, a stable cratonic area of Precambrian age (e.g., Chen and Jahn, 1998; Qiu et al., 2000). The Yangtze platform is situated between the Qinling–Dabie Mountain to the north, the South China block to the south and southeast and the Tibetan plateau to the west (Fig. 1). At present, the Yangtze platform, together with the South China block, represents a stable continental region that behaves as a rigid block, with only minor internal deformation (Wang et al., 2001; Calais et al., 2006; Zhang et al., submitted for publication), and lacks seismicity except at its margins (Schulte and Mooney, 2005).

The Yangtze platform is characterized by several first-order geophysical contrasts, including those seen in measurements of topography, crustal thickness, lithospheric thickness, and gravity (Fig. 1a). The topography decreases from an average surface elevation of 1000–2000 m in the western Yangtze to less than 500 m in the lower Yangtze (blue line in Fig. 1a). The thick (40–46 km) crust of the western Yangtze platform is separated from the thinner (30–36 km) crust of the eastern Yangtze platform and South Asia block by the north–south seismic belt (red lines in Fig. 1a; Li and Mooney, 1998; Li et al., 2006). A decrease in lithospheric thickness from greater than 200 km to ~80 km is evident at 110–112°E from surface wave tomography (dashed white line in Fig. 1a; Ma, 1987; Su et al., 1994; Huang et al., 2003; Lebedev and Nolet, 2003; Deng et al., 2004; An and Shi, 2006; Huang and Zhao, 2006). The Bouguer gravity field increases from −100 mGal to −40 mGal over a narrow band, forming a prominent north–south gravity lineament (transparent white strip in Fig. 1a; Ma, 1987; Yuan, 1996).

These geophysical anomalies divide Central China into a western and an eastern region. The western region is mainly dominated by crustal shortening and mountain building related to the India–Asia collision (e.g., Patriat and Achache, 1984; Dewey et al., 1989; Molnar et al., 1993; Royden et al., 2008). The eastern region has been affected by several tectonic processes, including: (1) clockwise rotation of the South China block during the Mesozoic (Meng et al., 2005), (2) widespread Cenozoic rifting and basaltic volcanism (Liu et al., 2004) and (3) east–west compression between the Pacific and Eurasian Plates (Ma, 1989; Ding, 1991).

In this paper we present the results from a seismic refraction/wide-angle reflection profile along the Yangtze River reaching from

* Corresponding author. Tel./fax: +86 10 82998313.
E-mail addresses: zhangzj@mail.iggcas.ac.cn (Z. Zhang), mooney@usgs.gov (W. Mooney).

0040-1951/$ – see front matter © 2009 Elsevier B.V. All rights reserved.
doi:10.1016/j.tecto.2009.05.022

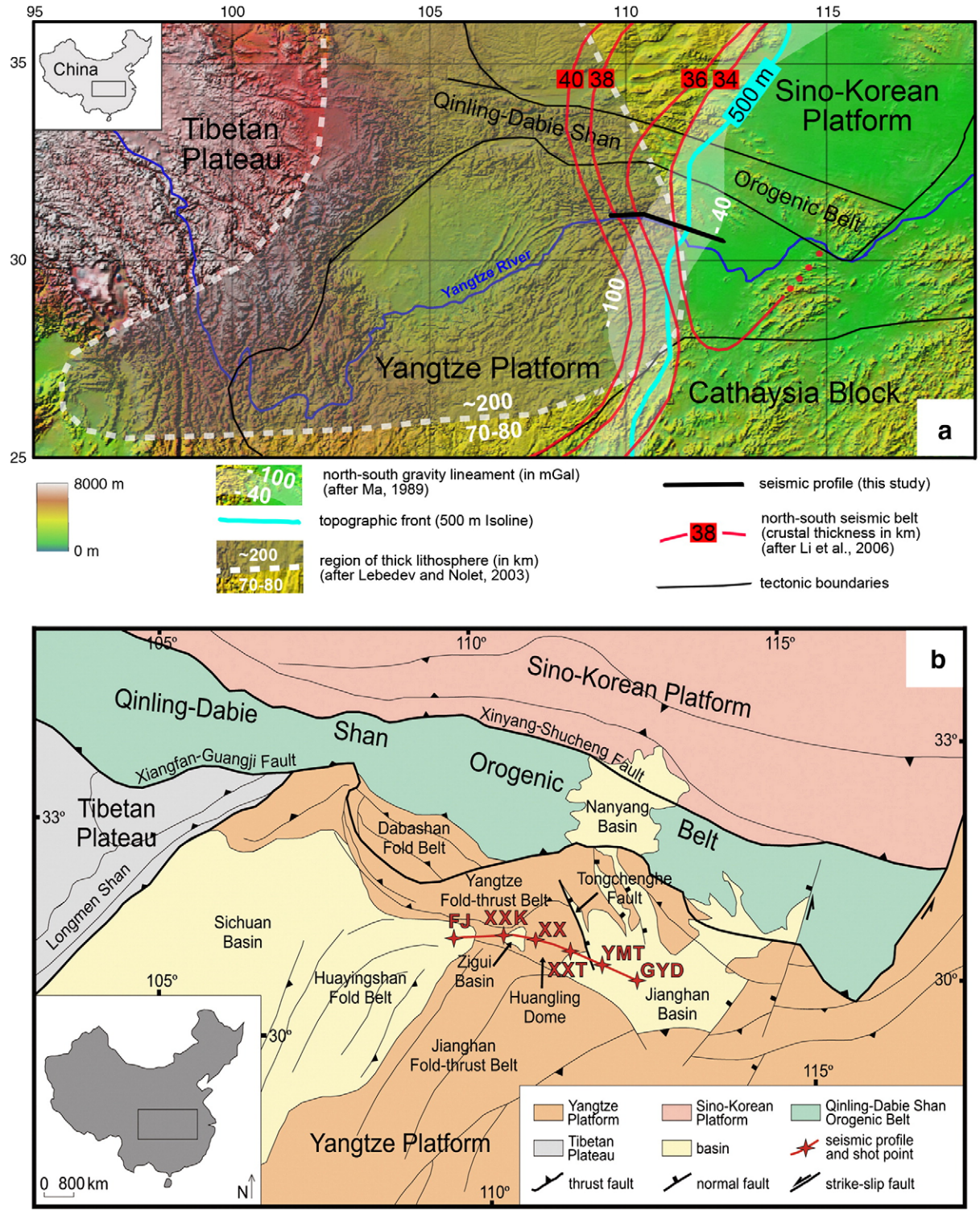

Fig. 1. (a) Topographic map of the study area with the Three Gorges area profile indicated as a thick black line. First order geophysical contrasts in topography, crustal thickness, lithospheric thickness, and gravity are indicated in different line patterns. Major tectonic units are shown with a thin black line. (b) Tectonic setting of the Three Gorges area illustrating the distribution of platforms, blocks, basins, sutures, major faults and major structural belts (modified from Liu et al., 2005). Stars indicate shot point locations. From west to east the shot points are FJ–Fengjie, GYD–Guanyingdang, XXK–Xixiankou, XX–Xianxi, XXT–Xiaoxita and YMT–Yuanmatou.

Fengjie (FJ), Sichuan Province, to Guanyindang (GYD), Hubei Province. The profile runs through the Three Gorges area, which is comprised of the Xiling Xia, Wu Xia, and Qutang Xia ("Xia" means "gorge" in Chinese). The field operations were carried out by the Institute of Dynamic Deformation and the Institute of Geophysics of the China Earthquake Administration during a period of 2 months.

2. Geologic background

The seismic profile presented here (Fig. 1a) lies on south of the Yangtze fold–thrust belt and north of the Jianghan fold–thrust belt (Fig. 1b). The local geology contains igneous and metamorphic rocks that range in age from Archean through to Late Proterozoic. The oldest

rocks are gneissic trondjhemites of Archean age that outcrop within the Huangling dome (Ames et al., 1996; Qiu et al., 2000).

Although the Yangtze platform stabilized after the Yangtze orogeny (~825 Ma), tectonic activity continued to affect the region. During the Silurian, the Yangtze platform collided with the Cathaysia fold belt to the south (Mattauer et al., 1985; Kenneth and Chen, 1999; Zhang and Wang, 2007). The South China block, including the Yangtze platform and the Cathaysia fold belt, consists of three Late Proterozoic through Mesozoic orogens from continental fragments sutured along two distinctive zones. This activity ended during the earliest Jurassic (Hsü et al., 1990). Additionally, the Yangtze platform collided along its northern margin with the Sino–Korean platform during the Early Triassic (Mattauer et al., 1985; Kenneth and Chen, 1999). This collision formed the Yangtze fold–thrust belt and the Jianghan fold–thrust belt (Fig. 1b), and produced strong deformation in the Three Gorges area.

Crustal extension (e.g. Ma and Wu, 1987) created fault-bound basins throughout the Three Gorges area (Fig. 1b). One of these basins, the Jianghan, is situated at the eastern extent of the seismic profile and is separated from the Huangling dome by the Tongchenghe fault, a northeast-dipping normal fault (Liu et al., 2003). The Jianghan basin resulted from regional extension accompanied by basement subsidence during the Cretaceous and Tertiary. Sediments that fill the Jianghan basin are non-marine and of Cretaceous to Quaternary age. These sediments are underlain by Yangtze platform sediments that include Early Mesozoic foreland basin sediments and a Late Precambrian–Early Triassic marine passive margin sequence (Wiener et al., 1997).

3. Seismic data

3.1. Seismic data acquisition and processing

The 300 km refraction/wide-angle reflection profile presented here runs from Fengjie, Sichuan Province, to Guanyingdang, Hubei Province. Explosive charges were fired at Fengjie (FJ), Xixiankou (XXK), Xianxi (XX), Xiaoxita (XXT), Yuanmatou (YMT) and Guanyingdang (GYD) (Fig. 1b). The first four charges were detonated at a water depth of 8–16 m; the two other charges were fired in drill-holes at a depth of 25 m. Explosive charge ranged from 1000 to 2000 kg. A total of 133 portable seismic stations were installed along the profile, including 100 single-vertical-component analogue seismographs and 33 three-component digital stations equipped with DZSS-1 seismographs. The receiver spacing was on average 2.2 km, with shot offsets ranging from 2 to 240 km. Analogue records provided by the magnetic tape recording were subsequently digitized at 5 ms intervals to be comparable with the digital record sections. A 1–10 Hz bandpass filter was applied to the plotted data. On all record sections, the acquired *P*-wave data have a high signal-to-noise ratio (Fig. 2a–f).

3.2. Correlation of phases

The *P*-wave phases referred to as P_g, P_2, P_3, P_4, P_mP and P_n were identified from the reduced *P*-wave record sections (Fig. 2).

The first arrival of P_g is a diving wave within the sedimentary layer or the crystalline upper crust. The maximum observed distance of the P_g phase varies for different shots, ranging from about 60 km to 110 km. The apparent velocity of the P_g waves is 5.8–6.2 km/s. P_g traveltimes are obviously delayed on shot gathers at YMT and GYD (Fig. 2e and f) compared to that on other shot gathers (Fig. 2a–d), which is consistent with the thick sediment of Jianghan basin.

Reflections from the top of the crystalline basement, cannot be identified. The phases P_2, P_3, and P_4 are reflections from intracrustal layers. All these phases have low energy, which indicates that there is a lack of strong, laterally consistent compositional layering in the crust.

P_mP is a strong reflection from the Moho and can be traced on the record sections for all shot points in an offset range of 100–200 km. P_mP reflections are concentrated in the offset range of 80–130 km west of shot point YMT, 150–200 km west of shot point GYD, and 120–180 km west of shot point FJ. This lateral variability observed in the P_mP reflections is an indication of lateral variations in crustal velocities, particularly in the lower crust.

P_n is the refracted wave through the upper mantle. This event can only be recognized on the east branch of FJ shot gather and the west branch of GYD shot gather (Fig. 2a and f). The apparent velocity of P_n varies along the profile with ~7.86 km/s at an offset range of 200–235 km east of shot point FJ and ~7.78 km/s at an offset range of 194–233 km west of shot GYD. This indicates the lack of a significant lateral variation in *P*-wave velocity within the uppermost mantle of the Three Gorges area.

3.3. Modeling data

The first step in our analysis was to get a reliable velocity model of upper crust. Usually, the seismic velocity structure of the upper crust has comparatively large lateral variations, so it is desireable to determine its structure in some detail. However this objective is not feasible by applying the standard RayInvr technique (Zelt and Smith, 1992) to the P_g data due to the small number of grid points in the RayInvr model. For this reason, we first have used a travel time inversion method based on finite differences (Vidale, 1988, 1990; Hole, 1992; Ammon and Vidale, 1993) to obtain *P*-wave velocities above the crystalline basement using P_g data. We initially assume a laterally homogeneous layered medium and invert the picked time-offset curves to derive one-dimensional velocity structures for all shots. These starting 1-D velocity models are sufficient to then perform an inversion for the 2-D velocity structure. After we have obtained a detailed 2D upper crust model from the inversion of P_g data, we use the RayInvr inversion technique in a layer-stripping approach (e.g., Zelt and Smith, 1992; Zelt and Forsyth, 1994; Zelt, 1999). It would be possible to determine a velocity model of the whole crust operating solely with the RayInvr technique from the beginning but its reliability would be lesser than following the two-step inversion procedure adopted here.

Velocity discontinuities across layer boundaries and vertical velocity gradients are thereafter adjusted by forward modelling to allow the best possible match with the observed amplitudes and travel times. This step is similar to the amplitude modelling described by Zelt & Forsyth (1994). Thus, travel time inversion and waveform modelling were alternated for each crustal layer until the best match to both data types (travel times and waveforms) was achieved. The observed seismic record sections, computed synthetic seismograms, ray path diagram, and the fit between the observed and the calculated travel time of the five SPs (shot points) were presented in the Figs. 3–7 respectively. The best fit between the observed and the calculated travel times for all *P*-wave phases is shown in Fig. 8a, and the subsurface ray coverage and the final two-dimensional crustal *P*-wave velocity model are presented in Fig. 8b and c, respectively. The ray path coverage of the profile (panel (b) in Fig. 8) suggests that most parts of our velocity model are well sampled by the seismic experiment.

The accuracy of the final crustal velocity model depends on the correct identification of the various phases, the density of rays, the shot point interval, and the receiver density. Seismic velocity determinations generally have lower errors than depth determinations. For the seismic data compiled here, seismic velocities are accurate to within 3% or ±0.2 km/s. All boundary depths, including the Moho, are accurate to within 10% of the stated depth (Mooney and Braile, 1989). Here, we present two sorts of model assessment.

(1) A direct model assessment technique was presented by Zelt & White (1995) in their study of the crustal structure of southeastern Canadian Cordillera, for which four additional inversions were performed based on different parameterization of the lower crust so

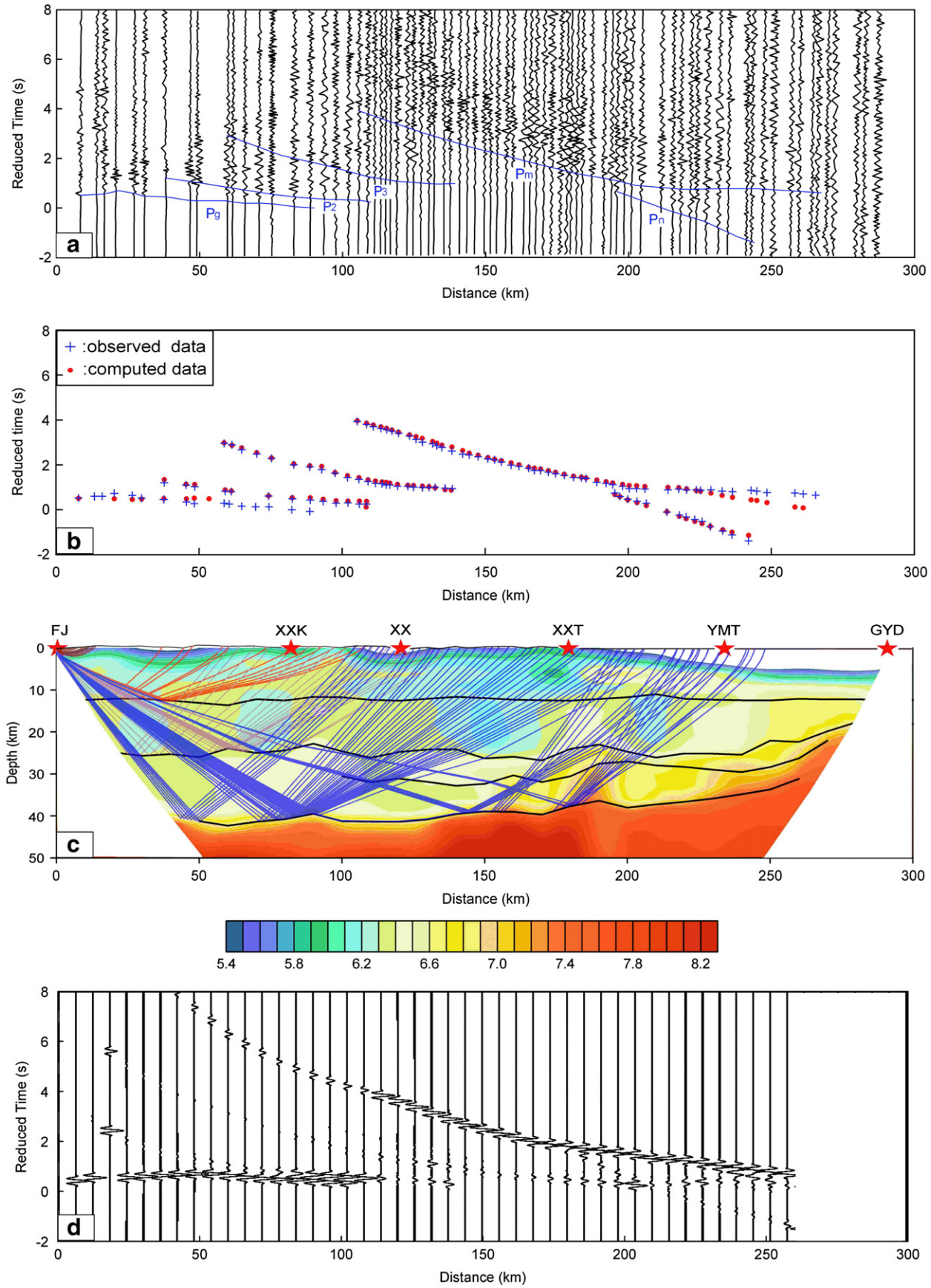

Fig. 2. (a) Seismic record section for the shot point Fengjie (FJ) in the Zigui platform fold belt; (b) the fit between the observed and the calculated travel time with the final crustal velocity model; (c) ray path diagram and (d) synthetic seismogram. The vertical axis indicates travel time reduced by 6 km/s.

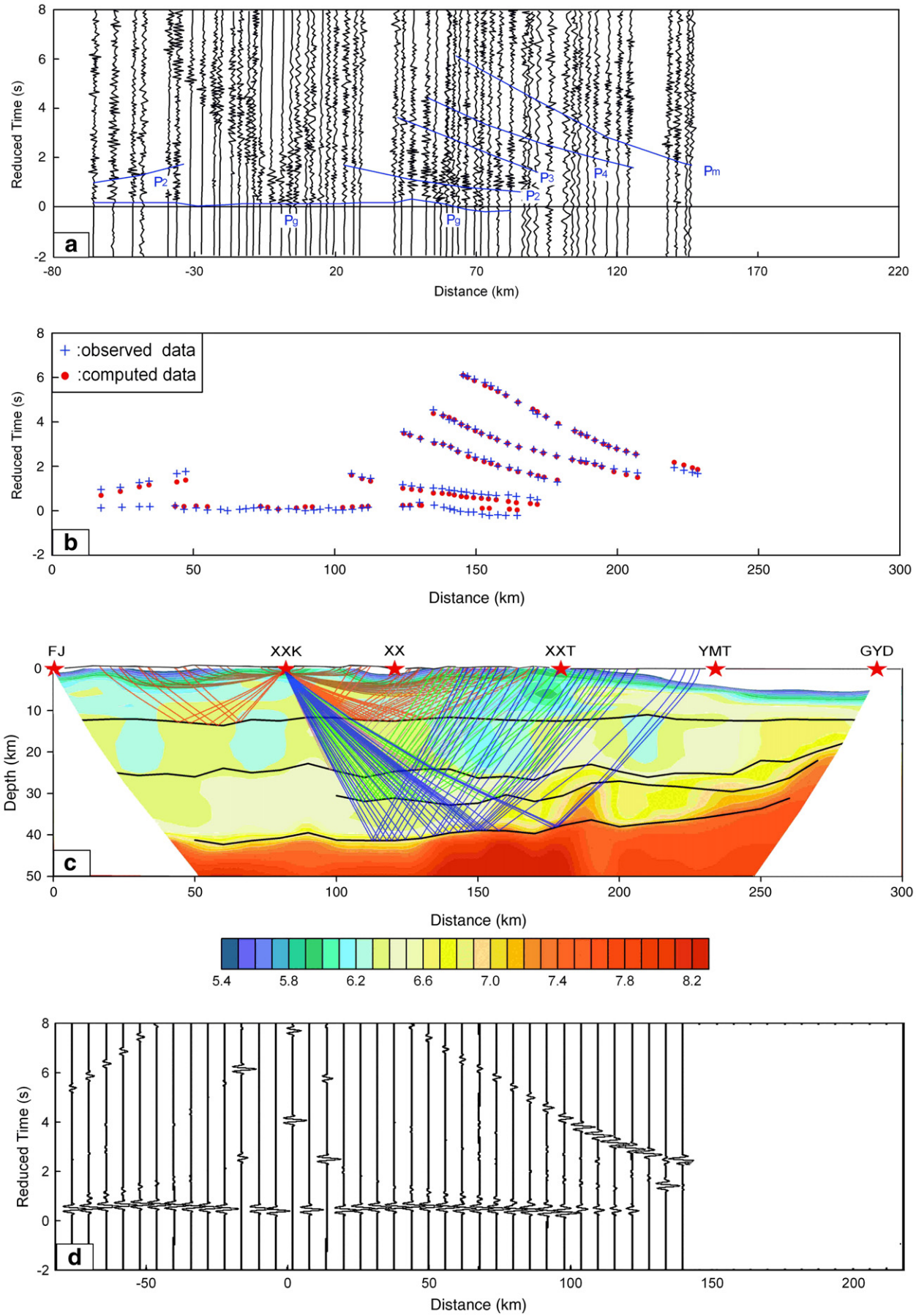

Fig. 3. (a) Seismic record section for the shot point Xixiankou (XXK) in the Zigui platform fold belt; (b) the fit between the observed and the calculated travel time with the final crustal velocity model; (c) ray path diagram and (d) synthetic seismogram. The vertical axis indicates travel time reduced by 6 km/s.

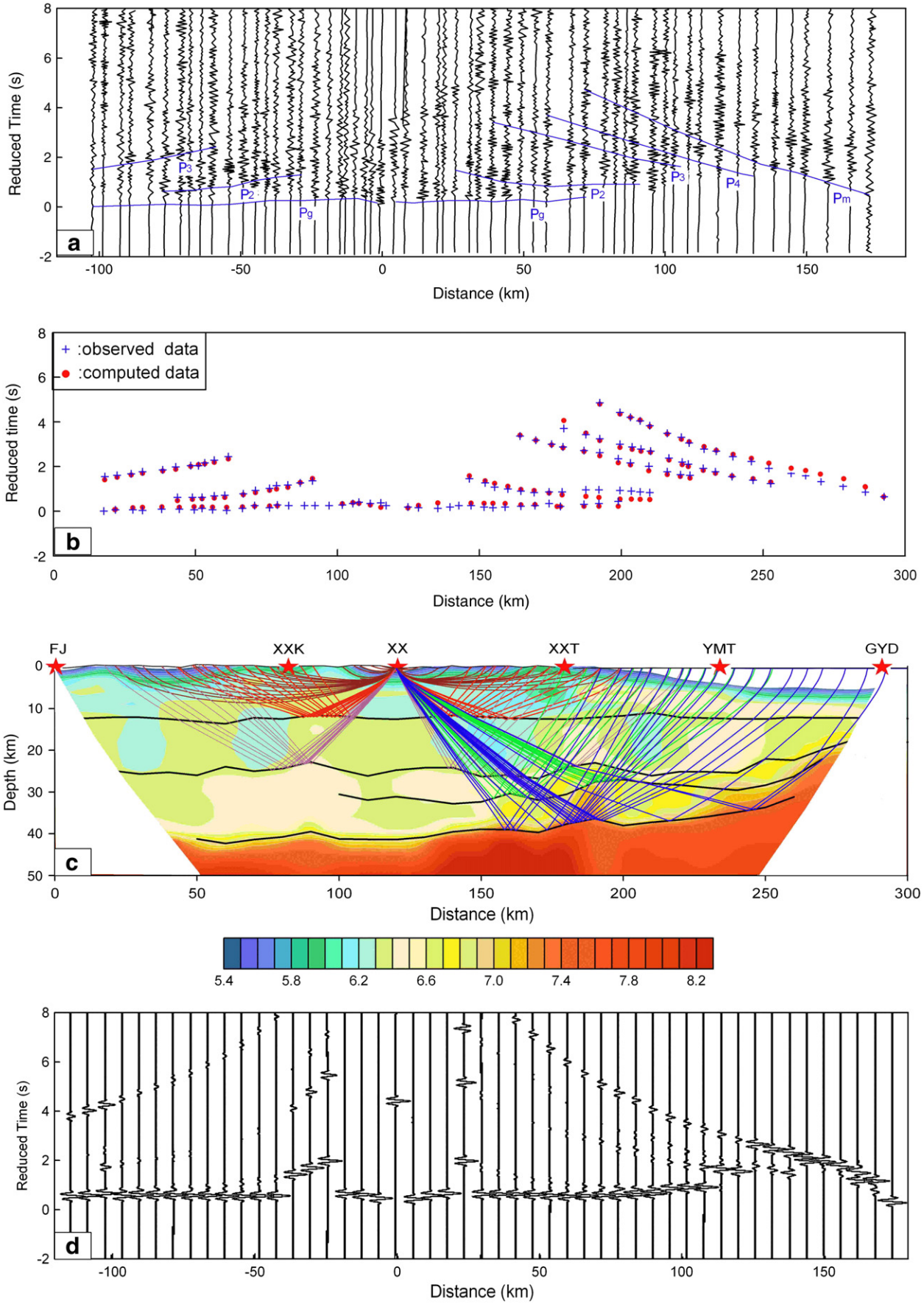

Fig. 4. (a) Seismic record section for the shot point Xianxi (XX) at the western end of the Huangling dome; (b) the fit between the observed and the calculated travel time with the final crustal velocity model; (c) ray path diagram and (d) synthetic seismogram. The vertical axis indicates travel time reduced by 6 km/s.

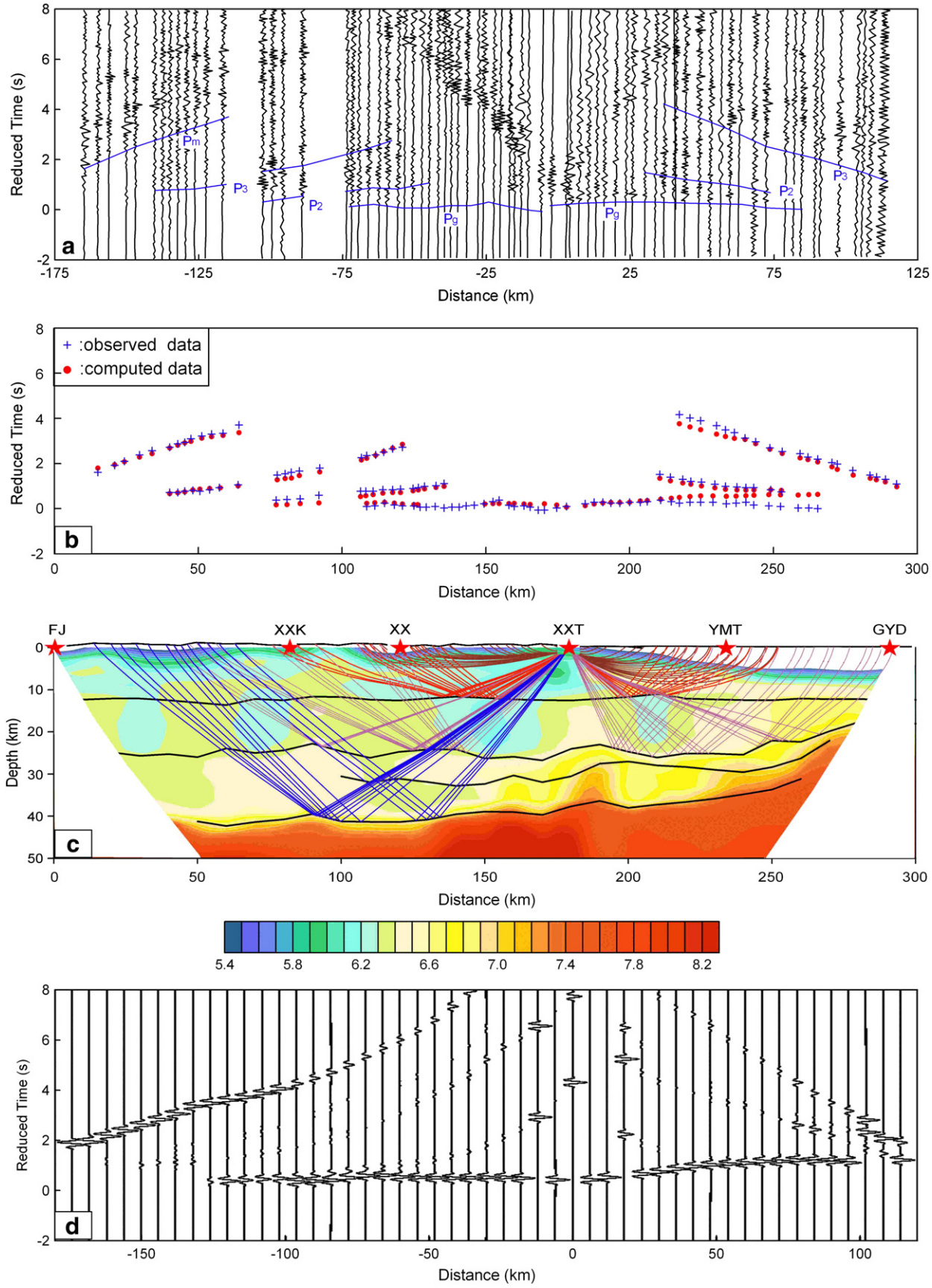

Fig. 5. (a) Seismic record section for the shot point Xiaoxita (XXT) in the Huangling dome; (b) the fit between the observed and the calculated travel time with the final crustal velocity model; (c) ray path diagram and (d) synthetic seismogram. The vertical axis indicates travel time reduced by 6 km/s.

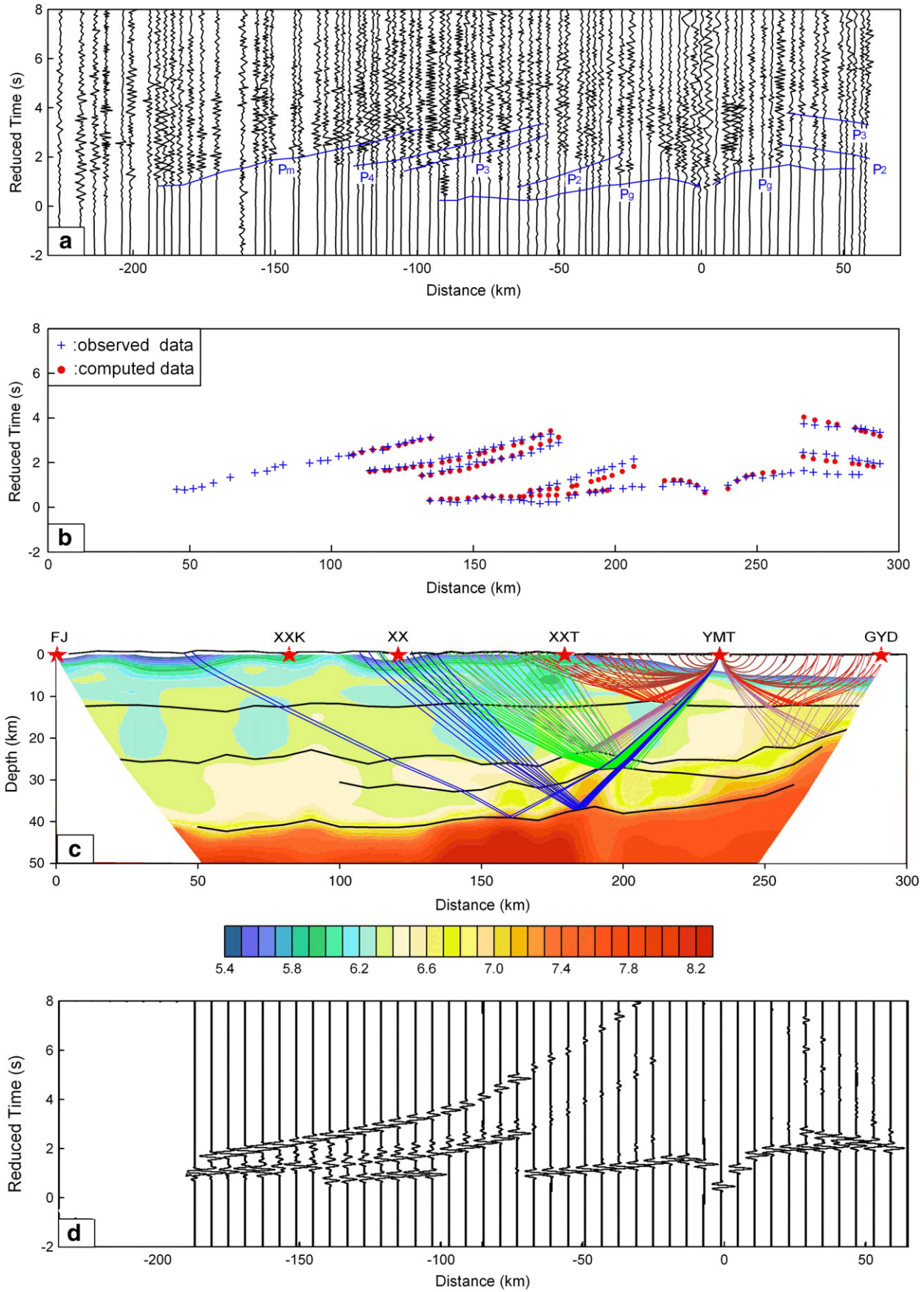

Fig. 6. (a) Seismic record section for the shot point Yuanmatou (YMT) in the Jianghan basin; (b) the fit between the observed and the calculated travel time with the final crustal velocity model; (c) ray path diagram and (d) synthetic seismogram. The vertical axis indicates travel time reduced by 6 km/s.

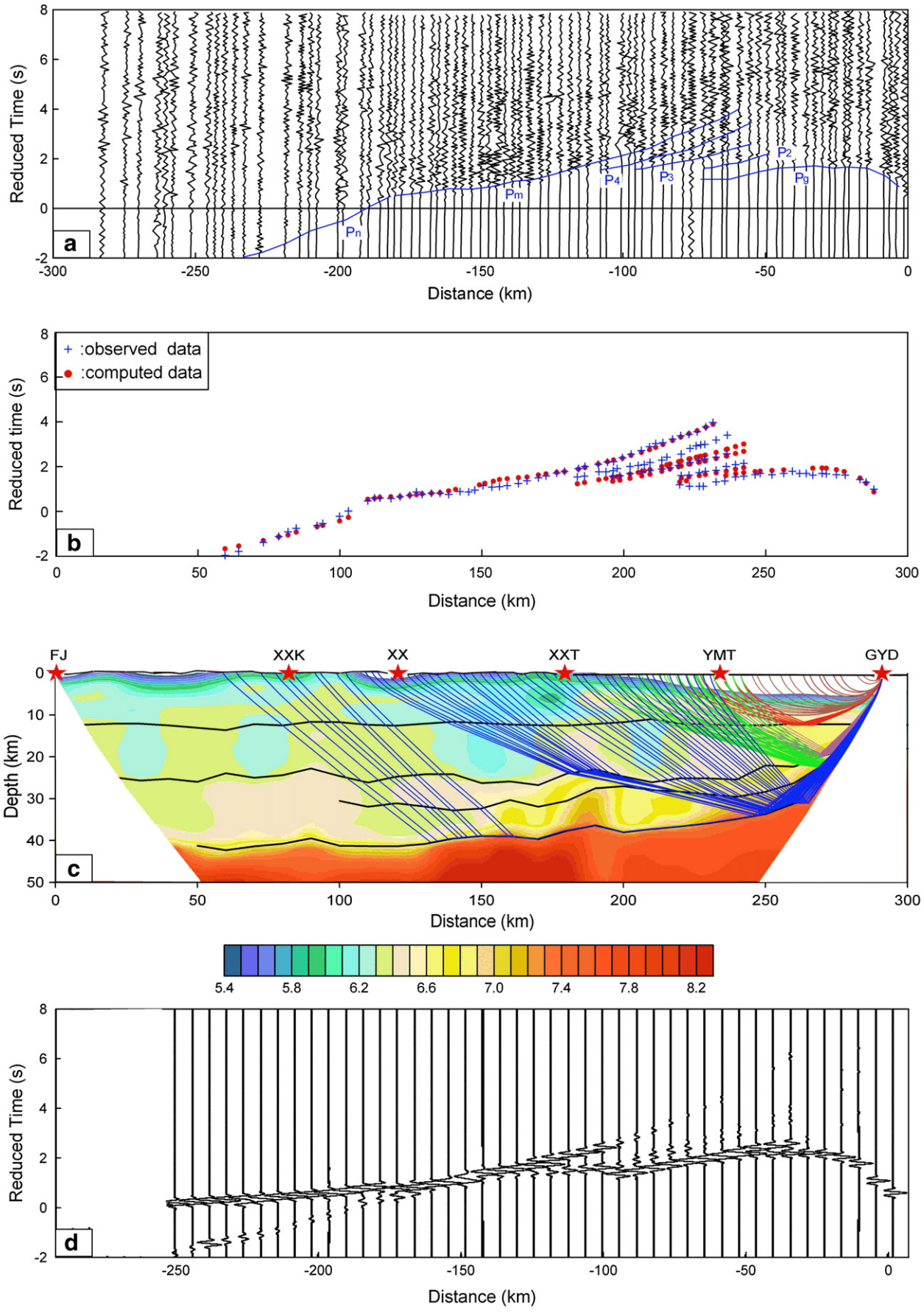

Fig. 7. (a) Seismic record section for the shot point Guanyingdang (GYD) in the Jianghan basin; (b) the fit between the observed and the calculated travel time with the final crustal velocity model; (c) ray path diagram and (d) synthetic seismogram. The vertical axis indicates travel time reduced by 6 km/s.

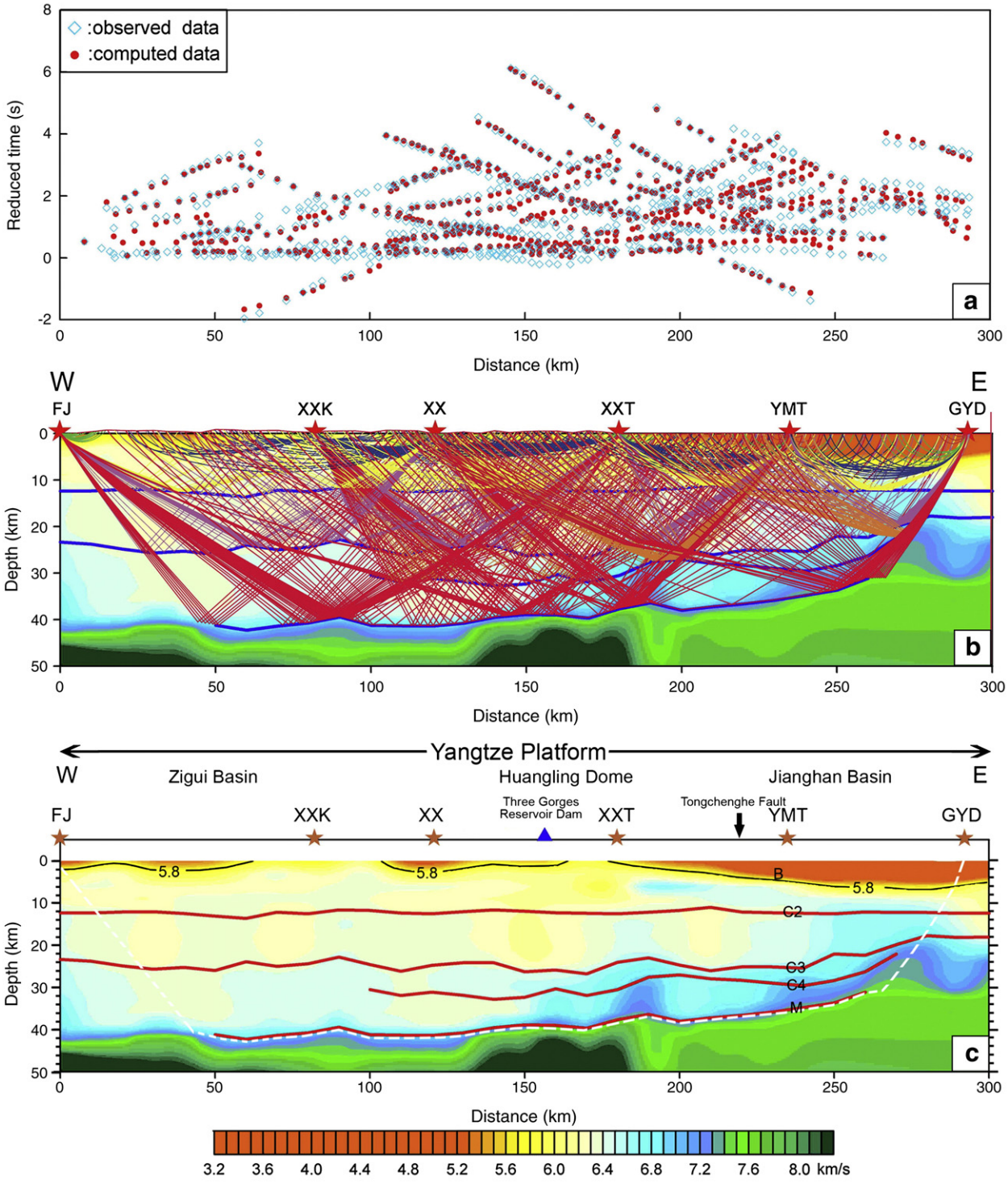

Fig. 8. Modeling results along the Three Gorges area profile reaching from Fengjie (shot point FJ) in the Zigui basin to Guanyingdang (shot point GYD) in the Jianghan basin. Stars indicate shot point locations. (a)Travel time fit: measured (marked with blue diamonds) and calculated (marked with red dots) travel times for shot point FJ, XXK, XX, XXT, YMT and GYD. The vertical axis indicates travel time reduced by 6 km/s. Travel times of all observed phases constitute the input data for ray tracing and synthetic seismogram. (b) Ray tracing and effective ray coverage: The vertical axis indicates depth in km. The thick blue lines represent interfaces determined by wide-angle seismic reflection data. (c) Final two-dimensional *P*-wave velocity model of the crust and uppermost mantle along the Three Gorges area profile with the tectonic setting shown above. The thick black line "B" indicates the 5.8-km/s-isoline and is assumed to mark the top of the basement. The thick red lines are interfaces determined by seismic wide-angle-reflection data, i.e., C2: base of upper crust, C3: base of middle crust, C4; base of upper layer of lower crust and M; base of the crust. The dashed white line indicates the area of dense ray coverage shown in Fig. 3b. The resulting velocity model is reliable inside the area of dense ray coverage; outside this area velocities are inferred due to requirements of the modeling program. (For interpretation of the references to colour in this figure legend, the reader is referred to the web version of this article.)

as to test the uncertainty of the derived multi-parameter. To test the robustness of crustal *P*-wave velocity model of Three Gorges, three other velocity inversions based on different parameterization were also employed to get a sense of the non-uniqueness of our preferred model (Fig. 9). The four models we have calculated represent: (a) our preferred velocity model (Fig. 9a), (b) an upper crust with strong lateral variation combined with a simple middle and lower crust that have constant velocity value (Fig. 9c), (c) an upper crust with strong

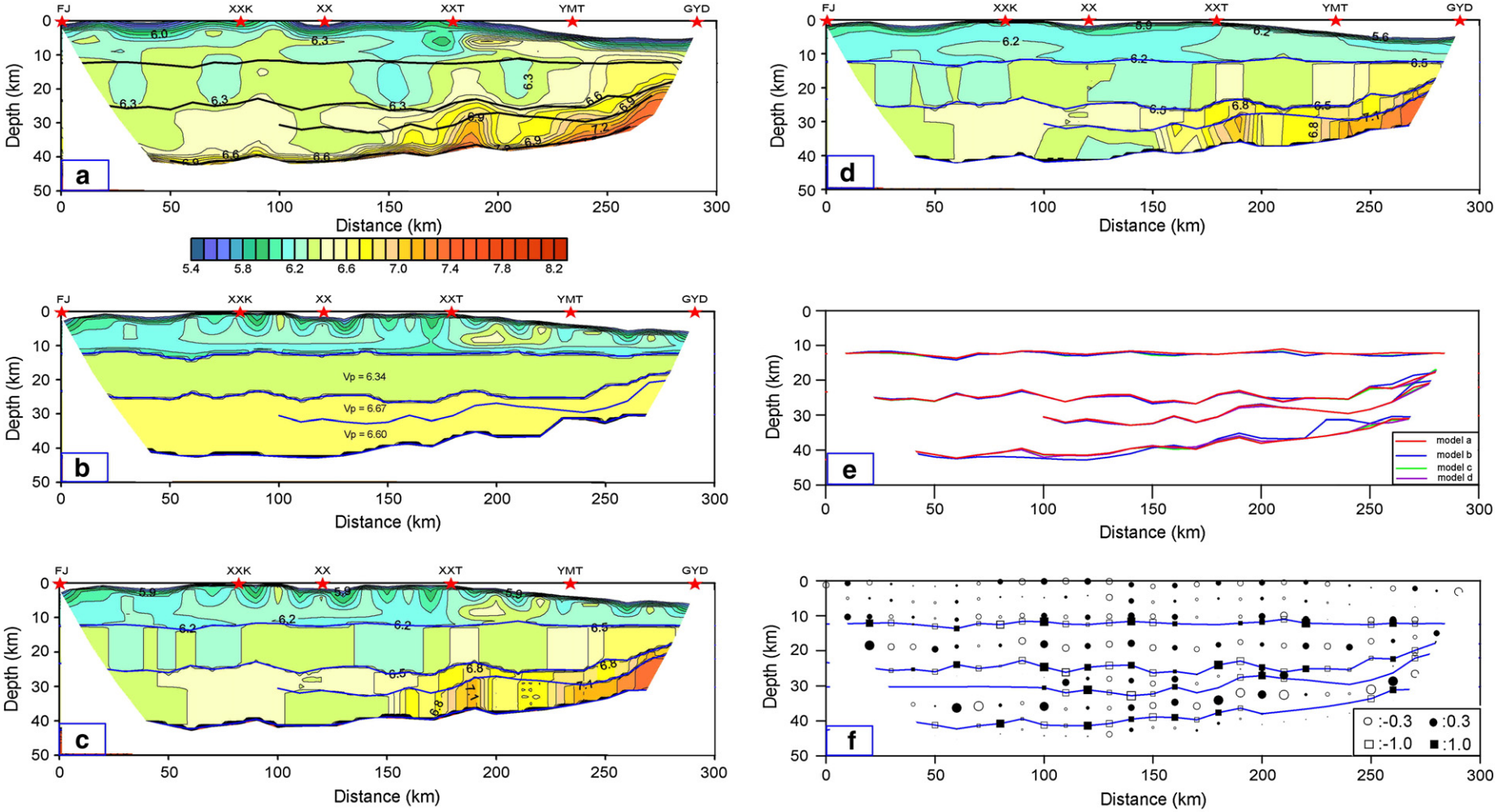

Fig. 9. Assessment of preferred and three alternative velocity models: (a) preferred velocity model, (b) alternative with an upper crust with strong lateral variation combined with a simple middle–lower crust which have constant velocity, (c) alternative with an upper crust with strong lateral variation combined with comparatively complex middle–lower crust, while the velocities along the bottom were equal to those of the top boundary, (d) alternative with an upper crust with comparatively smooth variation combined with complex middle–lower crust, (e) a close-up comparison of the boundaries from different alternative models, and the thick red line denotes our preferred model, (f) checkboard test of model (c), for which velocity perturbation of ± 0.3 km/s and depth perturbation of ± 1.0 km have been added to each velocity and depth node respectively so as to get a synthetic travel time data before inversion. (For interpretation of the references to colour in this figure legend, the reader is referred to the web version of this article.)

lateral variations combined with comparatively complex middle and lower crust, while the velocities along the bottom were equal to those of the top boundary, and (d) an upper crust with comparatively smooth variation combined with complex middle-lower crust (Fig. 9d).

It should be noted that to take advantage of the finite difference inversion, our preferred upper crust model has a more smooth geometry. Also, the shallow crust for the four models were generally similar, e.g., each exhibits an apparent low-velocity anomaly (LVA) beneath the SP XXT (Xiaoxita) and YMT (Yuanmatou), which accords with the Jiangling depression. An important issue is the validity of the lateral velocity variations of the middle and lower crust. Fig. 9 (c) and (d) show that they were in agreement with the features of our preferred model, e.g., these models also exhibit an obvious high velocity anomaly (HVA) on the west side of 200 km within the lower crust. Moreover, all boundaries were plotted together so as to assess the uncertainty of their geometry (Fig. 9e). The agreement of our preferred boundaries and those from other models indicates the robustness of our model.

2) Another useful and commonly applied inversion modeling assessment technique, the checkboard test, was employed to estimate the spatial model resolution (e.g., Zelt and Barton, 1998). To get a sense of lateral resolution of the preferred model, we first add velocity perturbations of ± 0.3 km/s to each velocity node, and depth perturbation of ± 1.0 km to each depth node in model (c). Then we compute the synthetic travel time data by forward modeling. Finally we invert this synthetic travel time data and thus get a calculated velocity and perturbation pattern (Fig. 9f). Our results show that around the center part of the profile the HVA (high velocity anomaly) and LVA (low-velocity anomaly) are alternatively distributed, and resemble the checkboard model. This suggests a lateral resolution of about 10 km within the centre part area of the profile.

3.4. Crustal P-wave velocity structure

The crustal *P*-wave velocity structure along the Three Gorges area seismic profile consists of five layers defined by the Earth surface and interfaces B, C2, C3, C4 and M (Fig. 8c). Interfaces C2, C3, C4 and M are interfaces determined by seismic wide-angle-reflection data and correspond to the P_2, P_3, P_4 and P_mP phases in Fig. 2. We lack evidence for a clear reflection from basement possibly due to the basement here being faulted/fractured. The five crustal layers are the low-velocity near-surface layer, the upper crust, the middle crust and a two-layer lower crust. We assume that the 5.8 km/s-isoline of the *P*-wave velocity model (B in Fig. 8c) marks the top of the crystalline upper crust.

The near-surface layer has velocities of 3.8–5.8 km/s and is composed of sediments and fractured basement rocks. West of shot point Xiaoxita (XXT), beneath the Zigui basin and the Huangling dome, the near-surface velocities vary between 5.4 and 5.8 km/s. West of shot point Xiaoxita (XXT), the 5.8 km/s-isoline (Fig. 8c) undulates in a depth range of 0–2 km, outlining local sedimentary basins. Beneath the Jianghan basin, which lies east to shot point XXT, *P*-wave velocities increase from 3.8 km/s near the surface to 5.8 km/s at a maximum depth of 6 km. The velocity contrast between the basin fill and basement outlines the two-dimensional structure of the Jianghan basin.

P-wave velocities within the upper crust vary between 5.8–6.3 km/s west of shot point XXT. East of shot point XXT, beneath the Jianghan basin, upper crustal velocities reach much higher values (5.8–6.6 km/s). Along the entire profile, the bottom of the upper crust is at a uniform depth of ~12 km. This 12 km thickness of the upper crust is a very typical value for continental crust (Mooney and Braile, 1989; Christensen and Mooney, 1995).

Beneath the Zigui basin and the Huangling dome, mid-crustal velocities vary between 6.3 and 6.4 km/s. Along this part of the profile, the bottom of the middle crust reaches a depth of 22–26 km. East of shot point YMT, beneath the northeastern margin of the Jianghan basin, the middle crust thins to a depth of only ~18 km beneath shot point GYD. In this part of the profile, middle-crustal velocities of 6.6–6.7 km/s are on average 0.3 km/s higher than velocities west of shot point YMT.

Beneath the Zigui basin, velocities within the lower crust are very low (~6.4 km/s). Typical lower-crustal values of 6.8 km/s are only reached a few km above the Moho. In contrast, beneath the Huangling dome and Jianghan basin the lower crust has seismic velocities of 6.8–7.2 km/s. Beneath the eastern segment of the profile, lower crustal velocities are ~0.3 km/s higher than beneath the western segment. Thus, lateral variation in lower-crustal velocities is similar to that found in the mid-crust.

Crustal thickness decreases along the profile from ~42 km beneath the Zigui basin in the west to ~30 km beneath the Jianghan basin in the east. Crustal thinning is accommodated by thinning of all crustal layers. The thickest upper, middle, and lower crystalline crust are found beneath the Zigui basin, with thicknesses of 10 km, 12 km and 17 km, respectively. The thinnest upper, middle, and lower crystalline crust are found under the Jianghan basin with thicknesses of 6 km, 6 km and 10 km, respectively. Beneath the Huangling dome, the seismic record sections of shot points XXK, XX, YMT and GYD (Fig. 2b, c, e and f) suggest a two-layered lower crust (interface C3 in Fig. 3c).

4. Discussion

The crustal thickness and *P*-wave velocity distribution along the Three Gorges area profile suggests a division of the crust into western and eastern regions (Fig. 8c). To further illustrate this we extracted velocity–depth functions for four locations along the profile and determined the average velocity of the crystalline crust (Fig. 10). Beneath the Zigui basin in the west, seismic velocity increases from 5.8 km/s at the top of the basement to 6.8 km/s at the base of the crust, with high velocity gradients at the top of the basement and at the base of the crust. The crystalline crust beneath the Zigui basin is characterized by low average velocities of about 6.36 km/s and a crustal thickness of ~40 km. In contrast, beneath the Jianghan basin at the eastern end of the profile, seismic velocity rapidly increases with depth, from 5.8 km/s at the top of the basement to 7.3 km/s at the base of the crust. Here, much higher average crustal velocities of 6.57 km/s or higher and a thin 30 km thick crust are evident.

The crustal thickness of ~42 km beneath the western segment of the profile (Zigui basin and Huangling dome) correlates well with the worldwide average of 41.5 km for shields and platforms. The average crustal velocity of about 6.36 km/s, however, is somewhat lower than the worldwide average of 6.42 km/s for shields and platforms (Christensen and Mooney, 1995). The crustal thickness of 30 km beneath the Jianghan basin at the eastern end of the profile is in good agreement with the continental global average for extended crust (30.5 km), but the average crustal velocities of 6.57 km/s and higher (even to 6.68 km/s) are much higher than the worldwide average of 6.21 km/s for extended crust (Christensen and Mooney, 1995). We interpret this high average crustal velocity to result from large-scale intrusion of mafic dikes and sills into the lower crust during the Cretaceous to Tertiary rifting that formed the Jianghan basin.

Grouping of *P*-wave velocities into intervals based on possible composition can be used to identify sedimentary ($V_p < 5.8$ km/s), felsic ($5.8 < V_p \leq 6.4$ km/s), intermediate ($6.4 < V_p \leq 6.8$ km/s), and mafic ($6.8 < V_p \leq 7.3$ km/s) material within the crust (Christensen and Mooney, 1995). These seismic velocities intervals to distinguish crustal composition are only global average values (Christensen and Mooney, 1995) and will vary with crustal composition and crustal temperature (Zhang et al., 2008). A comparison of these velocity intervals with the seismic velocity structure (Fig. 8c) suggests a clear compositional contrast between the western and eastern region of the profile. The Zigui basin and Huangling dome in the west are underlain by a felsic upper and middle crust and an intermediate

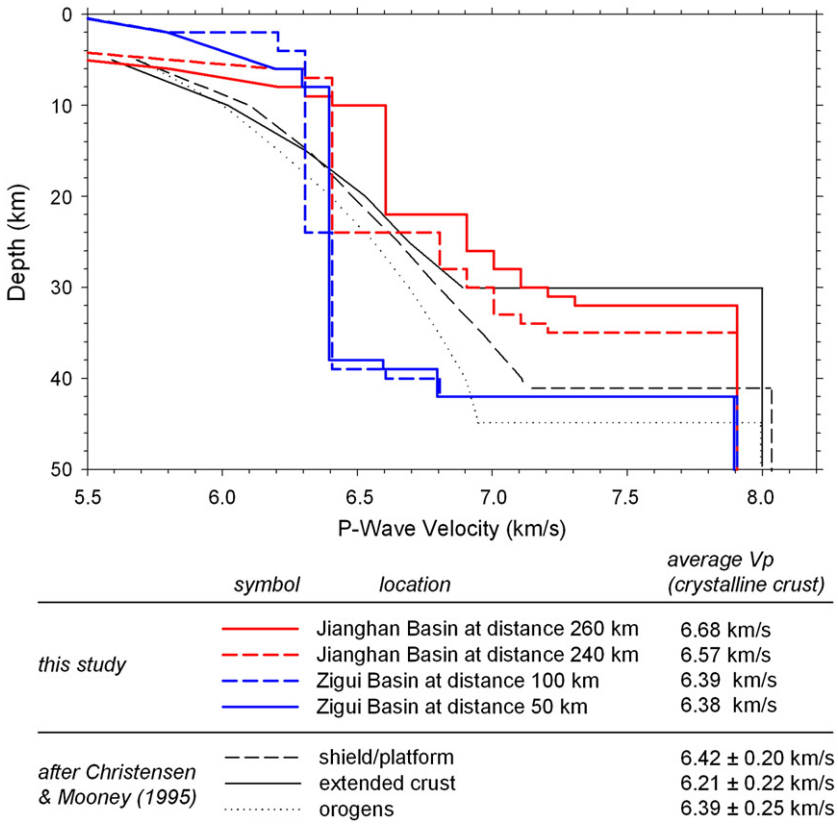

Fig. 10. *P*-wave velocity–depth function of the crust for locations in the Zigui basin and the Jianghan basin derived from the *P*-wave velocity model shown in Fig. 3c. Upper-mantle values of ~7.9 km/s are from tomographic studies (e.g., Hearn et al., 2004; Liang et al., 2004; Sun and Toksöz, 2006).

lower crust (Fig. 11). In contrast, the Jianghan basin in the east is composed of a felsic upper crust, an intermediate composition middle crust, and a mafic, possibly intrusively formed lower crust. Surface heat flow in the Yangtze platform is low, with mean values of ~49 mWm^{-2} in the Jianghan basin and ~53 mWm^{-2} in the Zigui basin and Huangling dome (Wang, 2001). This suggests that the

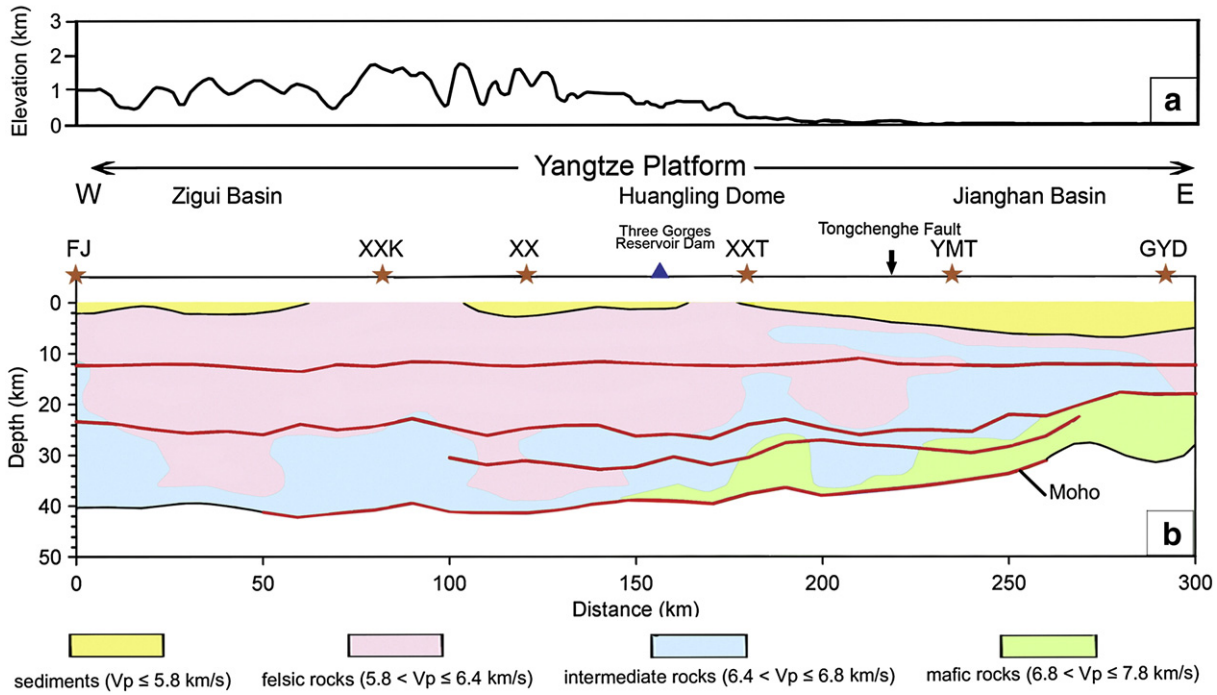

Fig. 11. (a) Topography and (b) compositional model of the crust along the Three Gorges area profile. The composition of the crust is derived from the *P*-wave velocity structure (Fig. 8c) using laboratory measurements of seismic velocities for a wide suite of rock types (Christensen and Mooney, 1995). The velocity intervals to identify sedimentary, felsic, intermediate and mafic composition are indicted in orange, pink, blue and green, respectively (after Christensen and Mooney, 1995).

variation in *P*-wave velocity between Jianghan basin, Zigui basin and Huangling dome is caused by compositional variation, rather than by elevated temperatures.

Previous seismic surveys have shown that a high velocity (>7.0 km/s) lower-crustal layer is generally absent beneath the Yangtze platform (Gao et al., 1998; Li and Mooney, 1998; Li et al., 2006). Our data confirm these observations for the Zigui and Huangling crust, but also demonstrate that the Jianghan basin has a mafic lower crustal layer that we attribute to mafic intrusion due to the Cretaceous to Tertiary rifting process that formed the basin. Seismic evidences of magmatic intrusions into lower crust are found in other active rift zones such as East Africa Rift (Birt et al., 1997; Thybo et al., 2000), central Denmark (Thybo et al., 2006) and Baikal Lake area (Thybo and Nielsen, 2009). Thybo et al. (2000) identified seismic reflections, which may be ascribed to magmatic intrusions into the lower crust in Kenya and argue that their presence may mask the true crustal thinning caused by the rifting processes. Similarly, a very high *P*-wave velocity of 7.3–7.5 km/s in the lowest crust of central Denmark was interpreted as mafic intrusion during the late Carboniferous and early Permian (Thybo et al., 2006). The observation of localized high velocity and highly reflective lower crust and Moho uplift beneath Baikal Lake were attributed to magma compensated crustal thinning (Thybo and Nielsen, 2009). The *P*-wave velocity of the uppermost mantle (P_n) is ~7.8 km/s, except for the area beneath the Huangling dome, where velocities reach much higher values of 8.0–8.3 km/s. Tomographic studies suggest upper mantle velocities of ~7.9 km/s (e.g., Hearn et al., 2004; Liang et al., 2004; Sun and Toksöz, 2006). We consider that the P_n velocity determined from tomographic studies, which used strong earthquakes as sources, is more reliable. Our measured P_n velocity in the topmost of upper mantle is 0.2–0.3 km/s lower compared to global average (Christensen and Mooney, 1995). The presence of a low-velocity mantle anomaly was also shown along the axis of the East African Rift Zone in Ethiopia (Bastow et al., 2005; Kendall et al., 2005). Our crustal velocity model and compositional model suggest Yangtze may have experienced rifting from lithosphere thinning.

5. Conclusions

We have determined the *P*-wave crustal velocity structure across the Three Gorges area in the western Yangtze platform along a 300 km-long seismic refraction/wide-angle reflection profile extending from the Zigui basin through the Huangling dome and into the Jianghan basin. The *P*-wave velocity model (Fig. 8c) suggests that the crustal structure changes significantly across the Tongchenghe fault at the transition from the Huangling dome to the Jianghan basin. West of the Tongchenghe fault, beneath the Zigui basin and the Huangling dome, we observe a ~42 km thick crust of somewhat low average crustal velocity (6.3–6.4 km/s). The interpretation of *P*-wave velocities into the composition (Fig. 11) suggests a dominantly felsic crust lying above an intermediate layer at its base. In contrast, east of the Tongchenghe fault, beneath the Jianghan basin, the 30 km thick crust is of high average velocity (6.6–6.7 km/s) and has a felsic-intermediate-mafic crustal layering. We interpret the high velocity lower crust as containing abundant mafic dikes and sills that were intruded during the Cretaceous to Tertiary rifting that formed the Jianghan basin.

In summary, our results suggest that, in addition to the first-order geophysical contrasts in gravity, topography, crustal thickness, and lithospheric thickness (cf. Fig. 1a), there also exists a pronounced west–east contrast in crustal structure and composition in the Yangtze craton along latitude ~30°N (Fig. 11).

Acknowledgment

The study was financially supported by the Chinese Academy of Sciences (KZCX2-YW-132), the National Nature Science Foundation of China (40721003, 40830315), and the Ministry of Science and Technology of China. The authors appreciate the field acquisition by the China Earthquake Administration. Comments by P.R. Reddy and N. Knepprath improved the text. Fig. 1b was made by N. Knepprath. We thank J.E. Vidale and C.A. Zelt for providing inversion software used in this study. Constructive suggestions from H. Thybo, J.E. Vidale and another anonymous reviewer improved the study.

References

Ames, L., Zhou, G., Xiong, B., 1996. Geochronology and isotopic character of ultrahigh-pressure metamorphism with implications for collision of the Sino–Korean and Yangtze cratons, central China. Tectonics 15, 472–489.
Ammon, C.J., Vidale, J.E., 1993. Tomography without rays. Bull. Seismol. Soc. Am. 83, 509–528.
An, M.J., Shi, Y.L., 2006. Lithospheric thickness of the Chinese continent. Phys. Earth Planet. Inter. 159, 257–266.
Bastow, I., Stuart, G., Kendall, J.M., Ebinger, C., 2005. Upper-mantle seismic structure in a region of incipient continental breakup: Northern Ethiopian Rift. Geophys. J. Int. 162, 479–493.
Birt, C.S., Maguire, P.K.H., Khan, M.A., Thybo, H., Keller, G.R., Patel, J., 1997. The influence of pre-existing structures on the evolution of the southern Kenya Rift Valley—evidence from seismic and gravity studies. Tectonophysics 278, 211–242.
Calais, E., Dong, L., Wang, M., Shen, Z., Vergnolle, M., 2006. Continental deformation in Asia from a combined GPS solution. Geophys. Res. Lett. 33, L24319. doi:10.1029/2006GL028433.
Chen, J., Jahn, B.M., 1998. Crustal evolution of southeastern China: Nd and Sr isotopic evidence. Tectonophysics 284, 101–133.
Christensen, N.I., Mooney, W.D., 1995. Seismic velocity structure and composition of the continental crust: a global view. J. Geophys. Res. 100, 9761–9788.
Deng, J.F., Mo, X.X., Zhao, H.L., Wu, Z.X., Luo, Z.H., Su, S.G., 2004. A new model for the dynamic evolution of Chinese lithosphere: 'continental roots-plume tectonics'. Earth-Sci. Rev. 65, 223–275.
Dewey, J.F., Cande, S., Pitman, W.C., 1989. Tectonic evolution of the India–Eurasia collision zone. Eclogae Geol. Helv. 82, 717–734.
Ding, G.Y., 1991. Relative motions of sub-plates and active blocks. Introduction to Lithospheric Dynamics of China. InSeismological Press, Beijing, pp. 142–153.
Gao, S., Zhang, B.R., Jin, Z.M., Kern, H., Luo, T.C., Zhao, Z.D., 1998. How mafic is the lower continental crust? Earth Planet. Sci. Lett. 161, 101–117.
Hearn, T.M., Wang, S., Ni, J.F., Xu, Z., Yu, Y., Zhang, X., 2004. Uppermost mantle velocities beneath China and surrounding regions. J. Geophys. Res. 109, B11301. doi:10.1029/2003JB002874.
Hole, J.A., 1992. Nonlinear high-resolution three-dimensional seismic travel time tomography. J. Geophys. Res. 97, 6553–6562.
Hsü, K.J., Li, J.L., Chen, H.H., Wang, Q.C., Sun, S., Şengör, A.M.C., 1990. Tectonics of South China: key to understanding west Pacific geology. Tectonophysics 183, 9–39.
Huang, J., Zhao, D., 2006. High-resolution mantle tomography of China and surrounding regions. J. Geophys. Res. 111, B09305. doi:10.1029/2005JB004066.
Huang, Z., Su, W., Peng, Y., Zheng, Y., Li, H., 2003. Rayleigh wave tomography of China and adjacent regions. J. Geophys. Res. 108, 2073. doi:10.1029/2001JB001696.
Kendall, J.M., Stuart, G., Ebinger, C., Bastow, I., Keir, D., 2005. Magma assisted rifting in Ethiopia. Nature 433, 146–148.
Kenneth, J.H., Chen, H.H., 1999. Geologic Atlas of China. Elsevier, Amsterdam. 362 pp.
Lebedev, S., Nolet, G., 2003. Upper mantle beneath Southeast Asia from S velocity tomography. J. Geophys. Res. 108, 2048. doi:10.1029/2000JB000073.
Li, S., Mooney, W.D., 1998. Crustal structure of China from deep seismic sounding profiles. Tectonophysics 288, 105–113.
Li, S., Mooney, W.D., Fan, J., 2006. Crustal structure of mainland China from deep seismic sounding data. Tectonophysics 420, 239–252. doi:10.1016/j.tecto.2006.01.026.
Liang, C., Song, X., Huang, J., 2004. Tomographic inversion of Pn travel times in China. J. Geophys. Res. 109, B11304. doi:10.1029/2003JB002789.
Liu, M., Cui, X., Liu, F., 2004. Cenozoic rifting and volcanism in eastern China: a mantle dynamic link to the Indo–Asian collision? Tectonophysics 393, 29–42.
Liu, S., Heller, P., Zhang, G., 2003. Mesozoic basin development and tectonic evolution of the Dabieshan orogenic belt, central China. Tectonics 22, 1038–1050. doi:10.1029/2002TC001390.
Liu, S., Steel, R., Zhang, G., 2005. Mesozoic sedimentary basin development and tectonic implication, northern Yangtze Block, eastern China: record of continent–continent collision. J. Asian Earth Sci. 25, 9–27.
Ma, X., Wu, D., 1987. Cenozoic extensional tectonics in China. In: Froidevaux, C., Kie, Tan Tjong (Eds.), Deep Internal Processes and Continental Rifting: Tectonophysics, vol. 13, pp. 243–255.
Ma, X.Y. (Ed.), 1987. Lithospheric Dynamics Map of China and Adjacent Seas (1:4,000,000) and Explanatory Notes. Geological Publishing House, Beijing.
Ma, X.Y., 1989. Atlas of Lithospheric Dynamics of China. China Cartographic Publishing House, Beijing, China. 70 pp.
Mattauer, M., Matte, P., Malavielle, J., Tapponnier, P., Maluski, H., Xu, Z.Q., Lu, Y.L., Tang, Y.Q., 1985. Tectonics of the Qinling Belt: build-up and evolution of Eastern Asia. Nature 327, 496–500.
Meng, Q.R., Wang, E., Hu, J.M., 2005. Mesozoic sedimentary evolution of the northwest Sichuan basin: implication for continued clockwise rotation of the South China block. Geol. Soc. Am. Bull. 117, 396–410. doi:10.1130/B25407.1.
Molnar, P., England, P., Martinod, J., 1993. Mantle dynamics, the uplift of the Tibetan Plateau and the Indian monsoon. Rev. Geophys. 31, 357–396.

Mooney, W.D., Braile, L.W., 1989. The seismic structure of the continental crust and upper mantle of North America. In: Bally, A.W., Palmer, A.R. (Eds.), The Geology of North America, An Overview. InGeological Society of America, Boulder, Colorado, pp. 39–52.
Patriat, P., Achache, J., 1984. India–Eurasia collision chronology has implications for crustal shortening and driving mechanism of plates. Nature 311, 615–621.
Royden, L.H., Burchfiel, B.C., van der Hilst, R.D., 2008. The geologic evolution of the Tibetan Plateau. Science 321, 1054–1058. doi:10.1126/science.1155371.
Qiu, Y., Gao, S., McNaughton, N.J., Groves, D.I., Ling, W., 2000. First evidence of >3.2 Ga continental crust in the Yangtze craton of south China and its implications for Archean crustal evolution and Phanerozoic tectonics. Geology 28, 11–14.
Schulte, S.M., Mooney, W.D., 2005. An updated global earthquake catalogue for stable continental regions: reassessing the correlation with ancient rifts. Geophys. J. Int. 161, 707–721.
Su, W., Woodward, R., Dziewonski, A., 1994. Degree 12 model of shear velocity heterogeneity in the mantle. J. Geophys. Res. 99, 4945–4980.
Sun, Y., Toksöz, M.N., 2006. Crustal structure of China and surrounding regions from P wave travel time tomography. J. Geophys. Res. 111, B03310. doi:10.1029/2005JB003962.
Thybo, H., Maguire, P.K.H., Birt, C., Perchuc, E., 2000. Seismic reflectivity and magmatic underplating beneath the Kenya Rift. Geophys. Res. Lett. 27 (17), 2745–2748.
Thybo, H., Sandrin, A., Nielsen, L., Lykke-Andersen, H., Keller, G.R., 2006. Seismic velocity structure of a large mafic intrusion in the crust of central Denmark from project ESTRID. Tectonophysics 420, 105–122.
Thybo, H., Nielsen, C.A., 2009. Magma-compensated crustal thinning in continental rift zones. Nature 457, 873–976. doi:10.1038/nature07688.
Vidale, J.E., 1988. Finite-difference calculation of travel times. B. Seismol. Soc. Am. 78, 2062–2076.
Vidale, J.E., 1990. Finite-difference calculation of traveltimes in three dimensions. Geophysics 55, 521–526.
Wang, Y., 2001. Heat flow pattern and lateral variations of lithosphere strength in China mainland; constraints on active deformation. Phys. Earth Planet. Inter. 126, 121–146.
Wang, Q., Zhang, P.Z., Freymueller, J.T., Bilham, R., Larson, K.M., Lai, X., You, X., Niu, Z., Wu, J., Li, Y., Liu, J., Yang, Z., Chen, Q., 2001. Present-day crustal deformation in China constrained by global positioning system measurements. Science 294, 574–577.
Wiener, R.W., Helwig, J.A., Rongpei, J., 1997. Seismic interpretation and structural analysis of a rifted thrust belt. Jianghan Basin. The Leading Edge, China, pp. 1177–1183.
Yuan, X., 1996. Atlas of Geophysics in China. Geological Publishing House, Beijing, China. 217 pp.
Zelt, C.A., Forsyth, D.A., 1994. Modeling wide-angle seismic data for crustal structure: southeastern Grenville province. J. Geophys. Res. 99, 11687–11704.
Zelt, C.A., Smith, R.B., 1992. Seismic travel time inversion for 2-D crustal velocity structure. Geophys. J. Int. 108, 16–34.
Zelt, C.A., White, D.J., 1995. Crustal structure and tectonics of the southern Canadian Cordilla. J. Geophys. Res. 100, 24255–24273.
Zelt, C.A., Barton, P.J., 1998. Three-dimensional seismic refraction tomography: a comparison of two methods applied to data from the Faeroe Basin. J. Geophys. Res. 103, 7187–7210.
Zelt, C.A., 1999. Modelling strategies and model assessment for wide-angle seismic travel time data. Geophys. J. Int. 139, 183–204.
Zhang, Z., Wang, Y.H., 2007. Crustal structure and contact relationship revealed from deep seismic sounding data in South China. Phys. Earth Planet. Inter. 165, 114–126. doi:10.1016/j.pepi.2007.08.005.
Zhang, Z., Zhang, X., Badal, J., 2008. Composition of the crust beneath southeastern China derived from an integrated geophysical data set. J. Geophys. Res. 113 (B4), B04417. doi:10.1029/2006JB004503.
Zhang, Z., Yuan, X., Chen, Y., Tian, X., Kind, R., Li, X., Teng, J., submitted for publication. The seismic structure of the Sichuan basin barrier to the east Tibetan escape flow. Earth Planet. Sci. Lett.